Traffic

© 2014 John Wiley & Sons A/S.
Published by John Wiley & Sons Ltd
doi:10.1111/tra.12182

Distinct Actions of Rab3 and Rab27 GTPases on Late Stages of Exocytosis of Insulin

Victor A. Cazares[1,2], Arasakumar Subramani[1], Johnny J. Saldate[1,2], Widmann Hoerauf[1,2] and Edward L. Stuenkel[1,2,*]

[1]Department of Molecular & Integrative Physiology, University of Michigan, Ann Arbor, MI 48109, USA
[2]Neuroscience Graduate Program, University of Michigan, Ann Arbor, MI 48109, USA
*Corresponding author: Edward L. Stuenkel, esterm@umich.edu

Abstract

Rab GTPases associated with insulin-containing secretory granules (SGs) are key in targeting, docking and assembly of molecular complexes governing pancreatic β-cell exocytosis. Four Rab3 isoforms along with Rab27A are associated with insulin granules, yet elucidation of the distinct roles of these Rab families on exocytosis remains unclear. To define specific actions of these Rab families we employ Rab3GAP and/or EPI64A GTPase-activating protein overexpression in β-cells from wild-type or Ashen mice to selectively transit the entire Rab3 family or Rab27A to a GDP-bound state. Ashen mice carry a spontaneous mutation that eliminates Rab27A expression. Using membrane capacitance measurements we find that GTP/GDP nucleotide cycling of Rab27A is essential for generation of the functionally defined immediately releasable pool (IRP) and central to regulating the size of the readily releasable pool (RRP). By comparison, nucleotide cycling of Rab3 GTPases, but not of Rab27A, is essential for a kinetically rapid filling of the RRP with SGs. Aside from these distinct functions, Rab3 and Rab27A GTPases demonstrate considerable functional overlap in building the readily releasable granule pool. Hence, while Rab3 and Rab27A cooperate to generate release-ready SGs in β-cells, they also direct unique kinetic and functional properties of the exocytotic pathway.

Keywords exocytosis, GTPase, insulin secretion, membrane fusion, Rab proteins

Received 16 April 2014, revised and accepted for publication 4 June 2014, uncorrected manuscript published online 6 June 2014, published online 26 June 2014

Insulin secretion from endocrine pancreatic β-cells is essential in regulating blood glucose levels. Key to this secretion is highly regulated membrane trafficking and exocytotic pathways of insulin-containing secretory granules (SGs). Defects in the process of insulin production, trafficking and secretion can lead to profound metabolic disorders and diabetes mellitus (1). Physiologically, insulin secretion is typically triggered from β-cells in response to elevated blood glucose concentrations, which raises the intracellular ATP/ADP concentration ratio and drives closure of K_{ATP} channels leading to a depolarization of the plasma membrane. Depolarization of the β-cell membrane then triggers activation of voltage-gated Ca^{2+} channels, wherein Ca^{2+} influx results in an induction of exocytosis of the insulin SGs (2). Prolonged glucose activation of β-cells induces a second sustained phase of exocytotic insulin secretion, the mechanisms of which are less well understood (3–6). In addition, incretins such as glucagon-like peptide-1 and glucose-dependent insulinotropic polypeptide strongly potentiate insulin secretion via cAMP signaling. Central to exocytosis of insulin SGs is the assembly/disassembly of molecular complexes that direct SG membrane targeting, tethering and biochemical competency for undergoing membrane fusion (7–9). While evolutionarily conserved SNARE proteins and regulators of SNARE complex assembly define the priming and fusion process, Rab GTPases are believed to be critical determinants of organelle identity, vesicle targeting, membrane tethering and SNARE complex formation (10,11).

Rab3A was the first Rab GTPase identified on insulin-containing SGs (12). Genetic studies using Rab3A knockout mice (13,14) as well as investigations examining

the effects of overexpression of Rab3A mutants (15–19) demonstrate that Rab3A is required for normal levels of insulin secretion and control of plasma glucose levels. More recently, Rab27A, a close evolutionary relative of Rab3, has also been found to be associated with these SGs (20–22). Similarly, functional studies of Rab27A-deficient mice (13,23,24) and overexpression of Rab27A mutants (21,25) have determined that Rab27A exerts regulatory activity over the exocytotic release of insulin. Although recent studies have confirmed that Rab3 and Rab27 are commonly colocalized on SGs and neuronal synaptic vesicles (26), the precise mechanisms by which they regulate late stages of exocytosis and the degree to which they exert functional overlap during vesicle priming and exocytosis remain poorly defined. Assigning specific roles to these Rabs has been complicated by their high structural homology and the promiscuity of effectors between the Rab3/Rab27 families. Moreover, knockout mice where three Rab3 isoforms are deleted do not survive when Rab3A is one of the deleted isoforms (14), further complicating studies assigning specific actions of Rab3 proteins versus Rab27 within the exocytotic pathway.

The subfamily of Rab3 consists of four isoforms (Rab3A–D), with each being present in pancreatic β-cells and in part associated with SGs (27). By comparison, Rab27 consists of two isoforms (Rab27A,B), but only Rab27A is expressed and targeted to insulin-containing SGs (24). The activity of Rab3 and Rab27 family proteins, like other GTPases, is determined by their cycling between a GDP-bound mostly inactive and cytosolic form and a GTP-bound active and membrane-bound form. Transitions between GTP/GDP states are mediated by guanine nucleotide exchange factors (GEFs) that stimulate the binding of GTP, and by GTPase-activating proteins (GAPs) that accelerate the intrinsic rate of Rab-GTP hydrolysis and return the Rab protein to an inactive state (28). While greater than 60 Rab proteins have been identified in mammalian cells, comparatively fewer regulatory Rab GEFs and Rab GAPs have been identified. Indeed, GTP binding of both Rab3 and Rab27 families is promoted by a single Rab GEF, termed Rab3GEP (29), suggesting a potential for commonality in their activation. Yet, return to a GDP-bound state for these Rabs is driven by distinct GAPs (Rab3GAP and EPI64, respectively) (30,31). Differences in regulated GAP inactivation likely lead to characteristic rates of GTP/GDP cycling and granule residency. Notably, fluorescence imaging of Rab3A and Rab27A on SGs has demonstrated that they exhibit kinetic differences in granule membrane association (26,32). For example, activation of secretion is often accompanied by rapid dissociation of Rab3A from the exocytic vesicles, while Rab27A appears to be largely maintained on SGs throughout fusion and early stages of endocytosis (33,34). These results are consistent with studies showing that association between Rab3 and the SG membrane is rigorously correlated with Rab3's GTP-bound state, while Rab27 appears to be able to associate with granules in both GDP- and GTP-bound states (35,36).

Multiple effectors have been reported for the Rab3 and Rab27 GTPases, which fall largely within four groups including, Rab-interacting molecules (RIMs and RIM-like proteins); synaptotagmin-like proteins (Slp and rabphilin); Slp-like proteins lacking C2 homologous regions (Slac and Noc2); and a vesicle priming protein Munc13-4 (37,38). For these effector families, RIM proteins interact with all isoforms of Rab3 but apparently not Rab27. Conversely, Slp1, Slp2-a, Slp3-a, Slp5 and Slac2-a–c interact specifically with Rab27A/B but not Rab3. By comparison, Slp4A, rabphilin and no C2 domain protein (Noc2) interact with Rab27A/B, Rab3s and Rab8 *in vitro*; however, binding affinities suggest preference for interaction with Rab27s *in vivo* (38,39). Finally, Munc13-4, a member of the Munc13 family that participates in exocytotic priming, has been reported to interact specifically with Rab27 (40). Importantly, Rab effectors may show cycling on/off membranes that differ kinetically from the Rabs themselves, suggesting that effector interactions with Rab GTPases may exhibit temporal and spatial differences and support distinct roles in the exocytic pathway (41). Although Rab3 and Rab27 are important regulators of secretory activity their functional specificity remains poorly understood, in part as a result of effector overlap.

In this study, we identify distinct roles of Rab3 and Rab27 family proteins in the final stages of the exocytotic pathway for insulin secretion from pancreatic β-cells. The investigations are novel in employing selective overexpression of the catalytic subunit of Rab3GAP and/or EPI64A to specifically activate GTP hydrolysis and respectively deactivate Rab3 and/or Rab27 family proteins. Whole-cell

capacitance measurements were used to evoke and measure exocytotic activity and to assign specific actions of the Rab families on functionally distinct vesicle pools of β-cells in pancreatic islet slices. Furthermore, we employed total internal reflection fluorescence (TIRF) microscopy of fluorescently tagged insulin-containing SGs to examine GAP overexpression effects on SG plasma membrane targeting and on juxtamembrane mobility. Our results provide the first quantitative evidence to distinguish largely differential roles of these Rab GTPase families in the priming of SGs into the immediately and readily releasable SG pools.

Results

To determine the sites of action and to differentiate distinct roles of Rab3 and Rab27 proteins on exocytosis in β-cells, experiments were performed using pancreatic islet slices from wild-type (wt) or Ashen mice. In addition, overexpression of GAPs, specifically Rab3GAP or EPI64A, was used to deactivate all isoforms of the Rab3 and/or Rab27 family, respectively. Islet slices, as opposed to isolated β-cells, were used to (i) retain the spatial and physiological characteristics of the exocytotic machinery and gap junctions of β-cells found in intact islet tissue; (ii) facilitate the maintenance of glucose responsiveness and electrical and secretory characteristics through organotypic tissue culture, while allowing efficient viral infection; and (iii) promote a tissue platform allowing stable long-term recording of membrane capacitance measurements from β-cells under a whole-cell voltage-clamp configuration.

As shown in Figure 1, cultured pancreatic islet slices allow effective infection with adenovirus for protein expression and provide excellent visualization of individual islet cells. The islet cell type specific to each electrophysiological recording was distinguished by measuring steady-state voltage-dependent inactivation properties of voltage-gated Na^+ channels. Mouse β-cells contain a voltage-gated Na^+ current whose steady-state inactivation properties are strongly left voltage shifted with respect to the inactivation properties of Na^+ currents of α- and δ-cells (Figure 1B) (42,43). The use of pancreatic islet slices also allows electrophysiological current-clamp recording of oscillations in electrical activity from individual β-cells, termed bursting, when the slices are exposed to stimulatory levels of glucose in the bathing media. Notably, this glucose-induced electrical bursting behavior was retained for at least 3

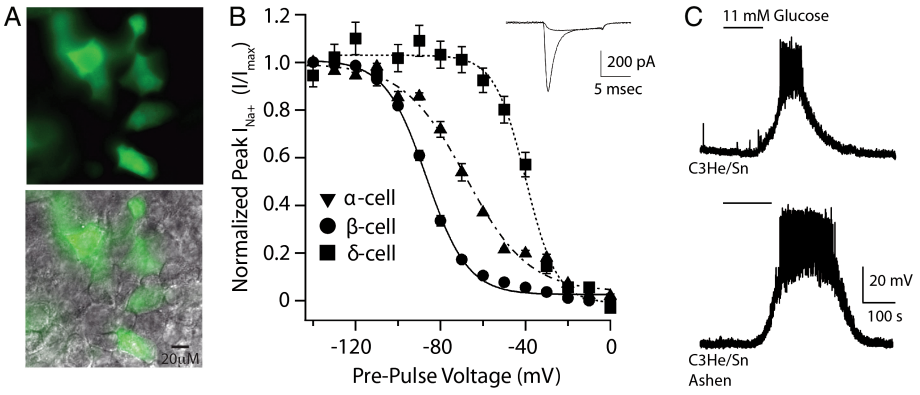

Figure 1: Adenoviral infection of pancreatic islet slices and electrophysiological identification of β-cells. A) Fluorescent micrograph of islet slice infected with pAdTrack-CMV-EGFP adenovirus (upper) that is overlayed on a differential interference contrast image of the slice (lower). B) Normalized averaged steady-state voltage-dependent Na^+ inactivation relationships recorded under voltage clamp from infected pancreatic islet cells (mean ± SEM; $N = \alpha$, 3; β, 8; δ, 3). Inactivation voltage-clamp protocol: holding potential, −70 mV; prepulse voltages of 200-millisecond duration ranged from −150 to 0 mV in 10-mV increments; pulse potential, 0 mV for 10 milliseconds; interpulse interval, 5 seconds. Inset, representative voltage-dependent current from β-cell when held at prepulse potentials of −100 and −40 mV. C) Current-clamp recordings of glucose-stimulated (11 mM) action-potential bursting behavior from β-cells in wt control (C3He/Sn) and Ashen islet slices that were subjected to 3 days organotypic tissue culture. Slices were perfused with normal extracellular solution containing 3 mM glucose for at least 5 min prior to glucose stimulation.

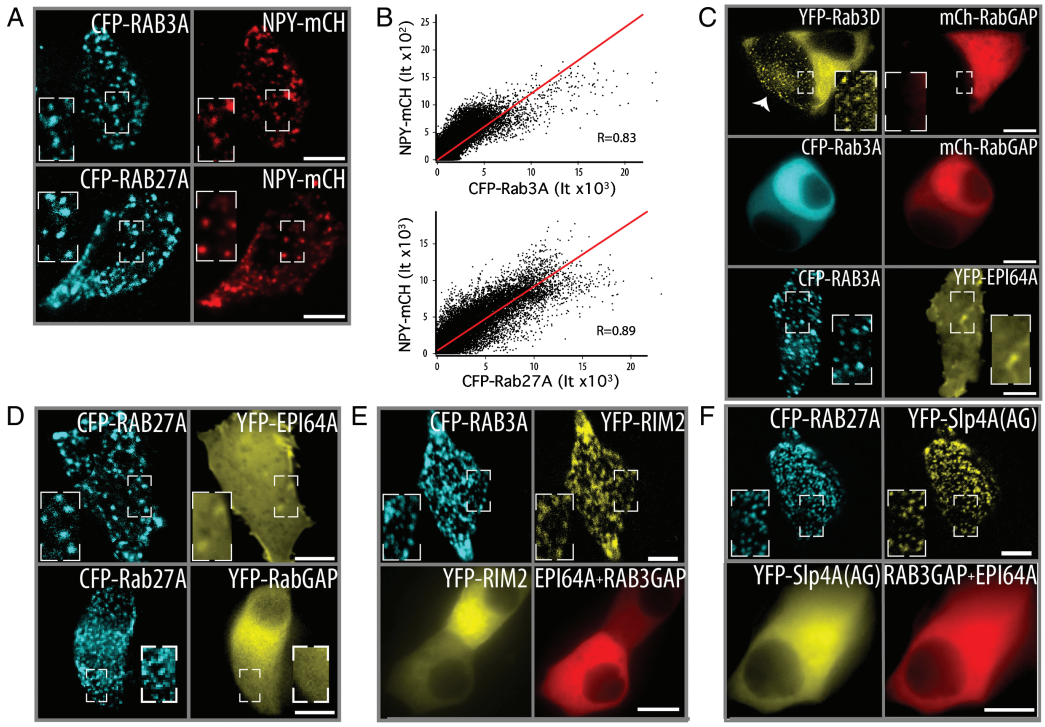

Figure 2: Expression of Rab GAPs transitions Rab3 and Rab27 into GDP-bound states. A) Confocal images of Min6 cells co-expressing CFP-Rab3A or CFP-Rab27A with a SG lumen marker (NPY-mCH). B) Cytofluorograms showing correlation of pixel by pixel intensities (It; $N = 4$ Rab3A; $N = 5$ Rab27A). C) Representative images of Rab3GAP and EPI64A co-expressed with Rab3A or Rab3D. Note that vesicular localization of Rab3D was retained in an adjacent non-Rab3GAP transfected cell (arrowhead). D) Co-expression of GAP proteins with Rab27A had no apparent effect on Rab27A's association with SGs. E) Co-expression of CFP-Rab3A + cYFP-Rim2α(1-179) demonstrates colocalization of punctate fluorescence (upper) that is lost with added expression of mCH-Rab3GAP (lower). F) Co-expression of CFP-Rab27A + cYFP-Slp4A(AGAAAY), denoted on figure as YFP-Slp4A(AG), demonstrates colocalization of punctate fluorescence (upper) that is lost with added expression of mCH-EPI64A (lower). Scale bar = 5 μm, within each figure insets show expanded view of a region of the cell (outlined in white-dashed line).

days in cultured slices, suggesting that normal phenotypic characteristics are maintained during organotypic slice culture on supported membranes (Figure 1C). Moreover, this glucose-induced bursting behavior was observed in cultures of slices from both wt and Ashen mice.

Rab3GAP and EPI64A have been characterized to exhibit Rab GAP activity specific to members of the Rab3 family and Rab27A (31,44). The effectiveness of overexpression of these GAPs to selectively shift the nucleotide-bound state of Rab3 or Rab27 proteins in insulin-secreting cells (Min6) was confirmed using a series of fluorescent imaging experiments (Figure 2). Notably, CFP-Rab3A or CFP-Rab27A expression exhibited punctate patterning of fluorescence that colocalized with a SG luminal reporter [neuropeptide Y (NPY)-mCH, Figure 2A] as confirmed by colocalization analysis (Figure 2B). Importantly, the punctate pattern of CFP-Rab3A or CFP-Rab3D was completely eliminated upon co-expression of mYFP-Rab3GAP but not with mYFP-EPI64A (Figure 2C). By comparison, punctate localization of CFP-Rab27A was retained upon co-expression of Rab GAPs (Rab3GAP or EPI64A, Figure 2D), a result consistent with reports indicating that Rab27A associates with SGs in both GDP- and GTP-bound states (35,36). To confirm that GAP overexpression effectively transitions these Rab GTPases into their GDP-bound state, irrespective of subcellular distribution, we next determined the effect of GAP overexpression on GTP-dependent Rab3A and Rab27A effector interactions (35). RIM2α(1-179) is a splice variant

that specifically interacts with GTP-bound Rab3 (18), whereas Slp4A(AGAAAY) is a mutant that interacts exclusively with the GTP-bound form of Rab27A (35). As shown in Figure 2E, co-expression of CFP-Rab3 and cYFP-RIM2α(1-179) results in colocalization of punctate fluorescence, which was lost when mCH-Rab3GAP was co-expressed. Co-expression of CFP-Rab27A with cYFP-Slp4A(AGAAAY) also demonstrated overlapping punctate fluorescence, which was lost with the added expression of mCH-EPI64A (Figure 2F). Taken together these results confirm that (i) Rab3GAP and EPI64A transition Rab3 and Rab27A, respectively, into their GDP-bound states; (ii) Rab27A localization to granules can be retained even in its GDP-bound form; and (iii) overexpression of GAPs strongly reduces Rab3 and Rab27A GTP-dependent effector interactions.

Docking of SGs at the plasma membrane is a key step in regulated exocytosis, as this is proposed necessary for the formation of *trans*-SNARE core complexes (vesicle priming). Not surprisingly, Rab3 and, more recently, Rab27 GTPases have been reported as central to targeting and docking secretory vesicles in β-cells (19,24), yeast (45), neuroendocrine cells [PC12 (46) and chromaffin cells (47)] and synaptic vesicles in *Caenorhabditis elegans* (48) and mammalian nerve terminals (49,50). Therefore, we next determined whether overexpression of the Rab GAP proteins exerted specific actions on insulin granule docking or on the mobility of insulin SGs directly adjacent to the plasma membrane. To assess effects of GAP overexpression on docking we used TIRF microscopy of a co-expressed SG luminal tag (NPY-mCH) in Min6 cells to visualize single SGs and quantify their density just beneath the plasma membrane. Min6 cells were used as they retain glucose-induced insulin secretion, aggregate in cell clusters and TIRF microscopy of β-cells in islet slices was not achievable. Representative images of NPY-mCH-tagged insulin SGs expressing only NPY-mCH or when co-expressed with Rab3GAP, EPI64A or with both Rab GAPs are shown in Figure 3A. As evident from the micrographs, no differences were observed in individual SG size or shape upon expression of the GAPs. In addition, SG density exhibited no significant differences between the different expression conditions (Figure 3B). These data differ from reported differences in SG docking observed with Rab3 and/or Rab27A knockdown (46,51,52) and

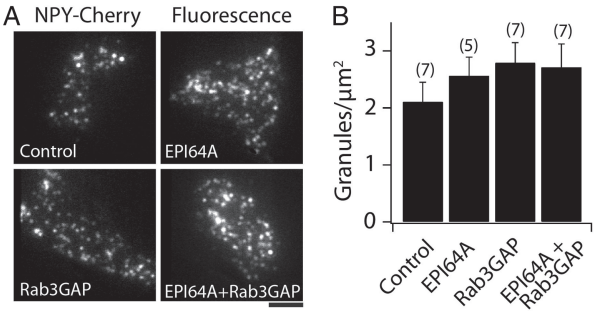

Figure 3: Overexpression of Rab GAP proteins does not alter density of SGs adjacent to plasma membrane. A) TIRF micrographs of SGs in Min6 cells transfected with NPY-mCH, a fluorescent lumenal marker of SGs, alone (control) or in combination with EPI64A (upper right), Rab3GAP (lower left) or EPI64A and Rab3GAP (lower right). B) Averaged measured density of SGs for each condition (mean ± SEM; *N* = number of cells). Scale bar below images = 5 μm.

suggest that Rab GAP overexpression, while strongly shifting nucleotide equilibrium of the associated GTPases to a GDP-bound state, may not completely preclude rapid passage of the GTPases through GTP-bound states to drive certain effector interactions important for SG docking.

Rab3 GTPases are believed to remain associated with docked SGs up until the final exocytotic steps leading to membrane fusion. By comparison, Rab27 may remain associated with vesicles throughout the exo-endocytotic process with its GTP/GDP nucleotide state being selectively regulated during passage through the exocytotic fusion and subsequent membrane recycling (35,36). While the functional role(s) of Rabs following granule tethering/docking are poorly understood, progression of vesicle priming following docking is commonly believed to lead to stable membrane association and an associated strong reduction in granule motion. Indeed, TIRF imaging of SGs immediately adjacent to the plasma membrane has repeatedly demonstrated that they are highly constrained in motion (53–57). To determine if a shift in nucleotide state equilibrium of Rabs may alone modulate motion of docked SGs we next performed time-lapse TIRF imaging of control and Rab GAP-transfected Min6 cells. Imaging was performed on cells held in physiological saline containing 3 mM glucose to reduce effects of secretion and activated granule recruitment on measures of docked

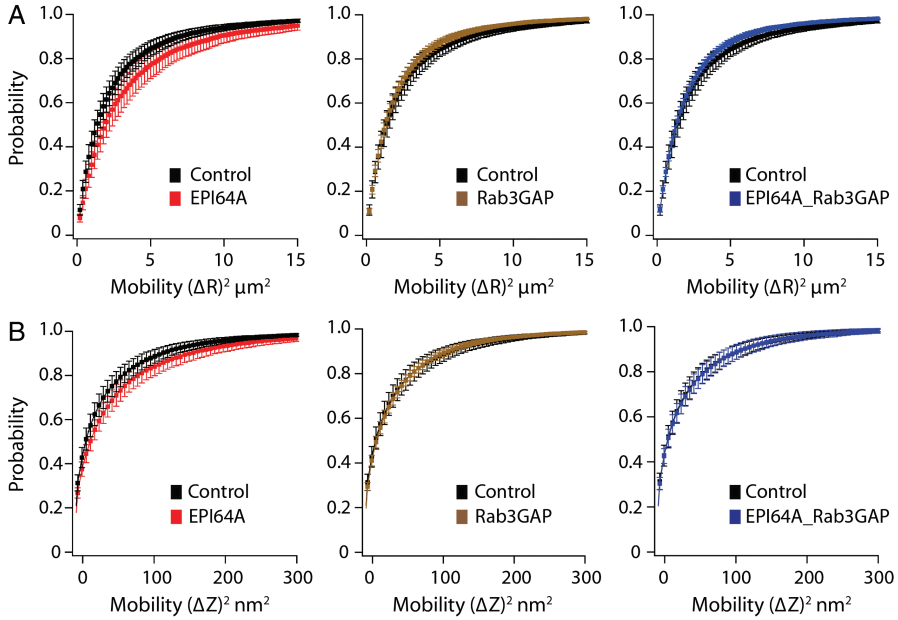

Figure 4: Mobility of membrane adjacent SGs is unaffected by overexpression of GAP proteins. A and B) Averaged cumulative probability distributions of apparent interframe fluctuations in central $x-y$ positions $(\Delta R)^2$ (A) or axial position $(\Delta Z)^2$ (B) of membrane adjacent SGs in Min6 cells transfected with the granule lumenal marker NPY-mCH and co-transfected with Citrine (control), Citrine–EPI64A, Citrine–Rab3GAP or Citrine–EPI64A + Citrine–Rab3GAP. The control $(\Delta R)^2$ and $(\Delta Z)^2$ data are included on each appropriate graph to allow comparison to the GAP treatments. Measurements made only on membrane adjacent SGs that were present throughout the entire 10-second imaging stream. Data are presented as mean ± SEM; control, 7 cells, 86 granules; EPI64A, 5 cells, 98 granules; Rab3GAP, 7 cells, 150 granules; EPI64A + RabGAP, 7 cells, 131 granules.

granule mobility. The $x-y$ $(\Delta R)^2$ and axial $(\Delta Z)^2$ mobility of individual docked SGs for each condition was determined. As shown in Figure 4, the measured $(\Delta R)^2$ and $(\Delta Z)^2$ cumulative probability of SG mobility in cells co-transfected with Rab3GAP, EPI64A or Rab3GAP + EPI64A, as well as NPY-mCH showed no significant differences from those of control cells (NPY-mCH only). These data suggest that Rab–effector interactions are not essential to maintenance of the stable and largely immobile population of docked SGs.

To identify specific Rab3 and Rab27A GTPase activities during the final steps of the regulated exocytotic pathway we employed highly time-resolved membrane capacitance (C_m) measurements from β-cells within islet tissue slices of wt control (C3H/He) or Ashen mice as well as from β-cells in the slices infected with Rab3GAP or EPI64A. Pancreatic β-cells contain well-described SG pools, including a large reserve pool (RP), a readily releasable pool (RRP), a small subset of the RRP termed the immediately releasable pool (IRP) and a highly calcium-sensitive pool (4,13,58–62). The IRP size is small and immediately released in response to a stimulus. If the stimulus is strong or prolonged and the IRP is depleted release then occurs from the RRP. The IRP is refilled from the RRP and the RRP from the RP. To elicit release and measure the size of the IRP and RRP a succession of step depolarizations (−80 mV holding potential to 0 mV step potential) was applied under whole-cell voltage clamp. Release and depletion of the IRP was accomplished by a series of five 50-millisecond step depolarizations, while the RRP was released using 10 500-millisecond step depolarizations, with each series using 100-millisecond interstep intervals. As Rab GTPases have been reported key for vesicle targeting, docking and priming we also determined the actions that Rab3 and Rab27A proteins exert on refilling of the IRP and RRP following their depletion. To measure Rab protein effects on refilling of the IRP and RRP a second train of successive step depolarizations was applied 20 seconds following cessation of the initial train of depolarizing stimuli.

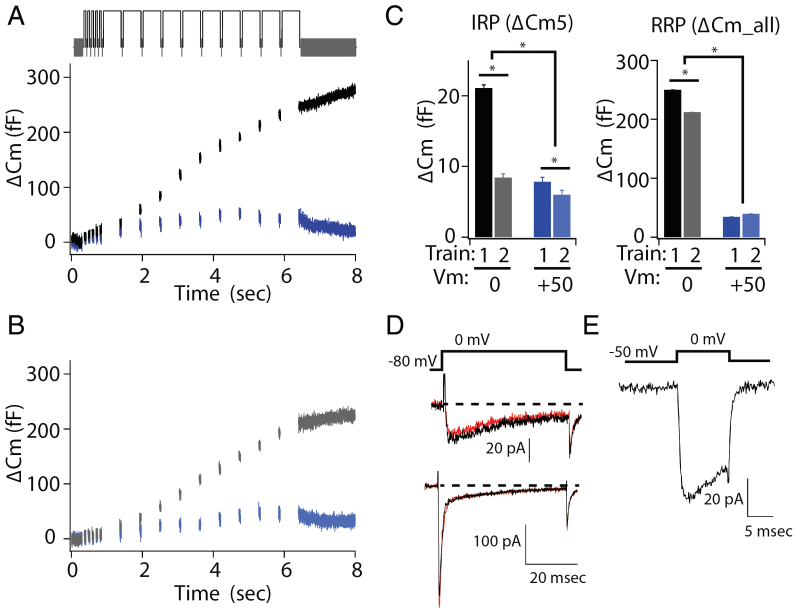

Figure 5: Determination of IRP and RRP size to sequentially applied step-depolarization pulse protocols in EGFP-infected β-cells. A) Averaged ΔC_m to applied pulse protocol from EGFP-infected cells. Depolarization steps were from a holding potential of −80 mV to 0 mV (black) or to +50 mV (blue). Pulse protocol pattern is illustrated above ΔC_m. B) Averaged ΔC_m to repeat application of pulse protocols (step to 0 mV, gray; +50 mV, light blue) applied to the same cells as in part A 20 seconds following the initial protocol. C) Averaged IRP (left) and RRP (right) pool sizes and recovery of granule pools following the 20-second non-stimulus interval. Mean ± SEM; $N = 19$ cells, 4 animals. D) Representative inward current to first step depolarization (holding potential −80 mV, step potential 0 mV) of initial (black) and second (red) applied pulse protocols. Currents from two different β-cells are shown (upper, lower) to illustrate interpulse interval protocol allows complete recovery of voltage-gated Ca^{2+} current (upper) and of Na^+ and Ca^{2+} current (lower). E) Averaged voltage-gated Ca^{2+} current from β-cells used for ΔC_m analysis measured on step to 0 mV from a holding potential (−50 mV) where voltage-gated Na^+ channels are inactivated.

In wt control β-cells, the first train of step depolarizations resulted in an averaged ΔC_m of 20 fF (fempto-Farads) corresponding to the IRP and 250 fF for the RRP (Figure 5A,C, black). Based on estimates of 1.7 fF per granule these ΔC_m values indicate IRP in control conditions to be ≈12 granules and the RRP to be ≈147 granules. Interestingly, these values for the IRP and RRP are approximately twice those we previously reported from isolated pancreatic β-cells (13), indicating that the more integrative character of islet slices likely retains more physiologically robust secretory responses in culture. Importantly, ΔC_m responses to a second train of step depolarizations applied 20 seconds after completion of the first train demonstrated only 45% recovery of the IRP while the RRP recovered to 85% of its initial value (Figure 5B,C, gray). This 20-second refilling interval, whereby incomplete refilling of the IRP and RRP was demonstrated in wt control cells, is used in the following experiments as a reference when evaluating effects of Rab protein nucleotide state on their capacities to direct SG pool refilling.

To confirm that the voltage-step-evoked ΔC_m of the β-cells reflect Ca^{2+}-dependent exocytotic activity we also tested for ΔC_m to successive step depolarizations from a −80 mV holding potential to +40 mV, a value closer to the expected Ca^{2+} equilibrium potential and strongly reduced voltage-gated Ca^{2+} current. As shown (Figure 5A–C, blue) steps to this potential resulted in significantly smaller evoked averaged ΔC_m response (9 fF IRP and 20 fF RRP).

Figure 5D compares representative macroscopic β-cell currents in response to the initial 50-millisecond voltage step during the first (black) and second (red) train of step depolarizations from −80 to 0 mV. Note that the

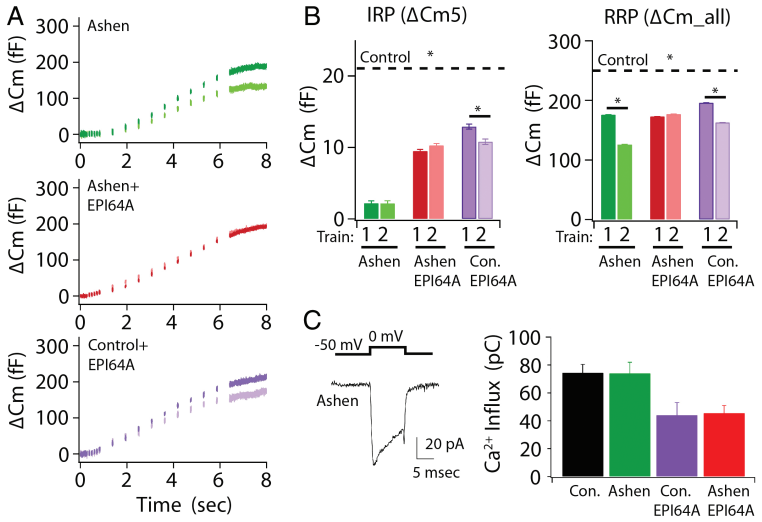

Figure 6: Rab27A is essential to development of IRP and key to defining RRP size in β-cells. A) Comparison of averaged ΔC_m to sequentially applied pulse protocols (20-second interval) from pAdTrack EGFP-infected Ashen β-cells (upper, green, $N = 22$ cells, 4 animals), pAdTrack EPI64A/EGFP-infected Ashen β-cells (middle, red, $N = 17$ cells, 3 animals) and pAdTrack EPI64A/EGFP-infected wt β-cells (lower, violet, $N = 11$ cells, 3 animals). ΔC_m to first applied protocol shown in darker color. B) Averaged size of IRP (left) and RRP (right) for each condition to each applied pulse protocol. Dashed line indicates average size of IRP and RRP to first pulse protocol under control conditions (EGFP-infected wt β-cells, Figure 4). Asterisk on dashed line indicates significance from conditions below. C) Averaged voltage-gated Ca^{2+} current (holding potential −50 mV, step potential 0 mV) from β-cells used for each ΔC_m analysis (left). Averaged time-integrated Ca^{2+} influx (pC) for each condition as measured from inward current evoked on step to 0 mV from −50 mV holding potential (right, N = control, 11; Ashen, 15; Ashen + EPI64A, 8; control + EPI64A, 3).

current responses to each applied train were equivalent, suggesting that differences in ΔC_m responses between the trains are not the result of inadequate recovery or of rundown of the evoked current. Most of the β-cells demonstrated a rapid inward followed by a strongly reduced sustained inward current following the step depolarizations that likely reflect voltage-gated Na^+ and Ca^{2+} current components (Figure 5D, lower). Interestingly, in a small subset of β-cells only the sustained current, most likely representing Ca^{2+} influx, was observed, which also demonstrated complete recovery during the intertrain interval (Figure 5D, upper). Indeed, voltage steps to 0 mV from a −50 mV holding potential, where voltage-gated Na^+ channels in β-cells are inactivated, resulted in a sustained inward Ca^{2+} current with amplitudes close to that of the sustained current observed upon steps to 0 mV from a −80 mV holding potential (Figure 5E).

Insulin-containing SGs in wt control β-cells possess both Rab27A and the four isoforms of Rab3 (A, B, C and D) GTPases (20–22, 63, 27). As a test for distinct as well as complimentary actions of these GTPases we initially examined the effects of Rab27A on IRP and RRP sizes and on pool refilling using three separate experimental conditions. These conditions include exocytotic measurements from β-cells in islet slices of the Ashen mouse (i.e. Rab27A-deficient) and of β-cells following EPI64A adenoviral infection of islet slices isolated from Ashen and wt mice. As shown in Figure 6, the averaged initial IRP and RRP exocytotic responses measured from β-cells under each of these three conditions were significantly reduced from those of wt mice (control response, dashed line, Figure 6B). The IRP from β-cells of Ashen mice was most strongly affected (~90% reduction), whereas overexpression of EPI64A in β-cells of Ashen or wt control slices resulted in an approximately 50% reduction in IRP from control. The reduced effect on IRP size with EPI64A overexpression in Ashen β-cells suggests that EPI64A exerts Rab27A-independent effects on secretion. Indeed, EPI64A has also been characterized as a binding protein of EBP50,

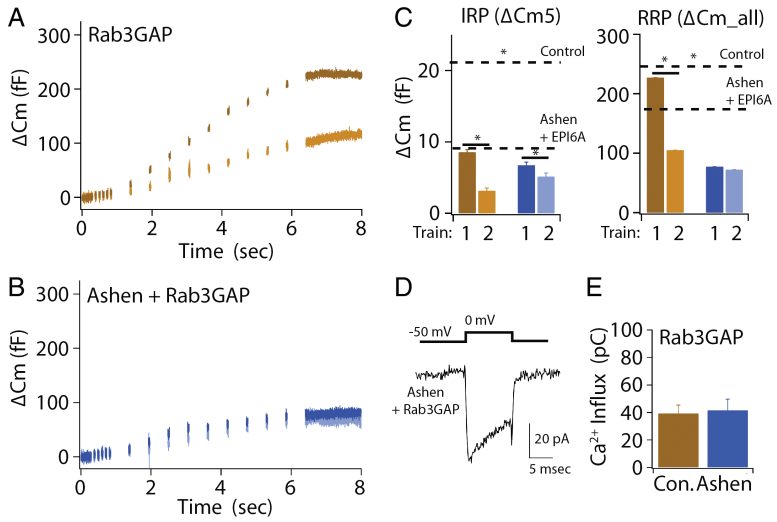

Figure 7: Rab3 exerts a central role in rapid refilling of RRP in β-cells. A) Comparison of averaged ΔC_m to sequentially applied pulse protocols (20-second interval) from pAdTrack Rab3GAP/EGFP-infected wt β-cells (brown, $N = 15$ cells, 4 animals), with darker color showing data from first pulse protocol. B) Averaged ΔC_m responses from pAdTrack Rab3GAP/EGFP-infected Ashen β-cells (blue, $N = 15$ cells, 3 animals). Darker color shows data from first pulse protocol. C) Averaged size of IRP (left) and RRP (right) for each condition determined from each applied pulse protocol. Dashed lines indicate average size of IRP and RRP to first pulse protocol under control conditions (EGFP-infected wt β cells) and in Ashen cells. D) Averaged Ca^{2+} current from Ashen β-cells infected with pAdTrack Rab3GAP/EGFP used for ΔC_m analysis. E) Averaged Ca^{2+} influx (pC) for β-cells from wt (control) and Ashen mice infected with pAdTrack Rab3GAP/EGFP (N = control + Rab3GAP, 5; Ashen + Rab3GAP, 9).

which participates in actin bundling at the cell periphery (64). By comparison to the substantial reduction of the IRP from wt control with loss of Rab27 or Rab27-GTP, the RRP for each condition (Ashen, Ashen + EPI64A and control + EPI64A) was significantly reduced, but only by approximately 25%. Note that measured differences in IRP and RRP pool sizes of control and Ashen β-cells were not associated with changes in voltage-gated integrated Ca^{2+} influx (Figure 6C). Moreover, while expression of EPI64A resulted in a reduced Ca^{2+} influx, diminution in ΔC_m responses was not greater than observed for Ashen-only β-cells.

Rab27A effects on refilling of the IRP and RRP were determined through application of a second train of step depolarizations following a 20-second recovery interval. Measurement of the ΔC_m responses showed that in Ashen β-cells the reduced IRP completely refilled, while the RRP refilled to approximately the same percentage as observed for wt β-cell controls (Figure 6B). By comparison, Ashen β-cells overexpressing EPI64A demonstrated complete refilling of both the IRP and RRP, whereas the overexpression of EPI64A in control cells led to incomplete refilling of the IRP and RRP. EPI64A facilitation of RRP pool refilling in the absence of Rab27A, but not in Rab27A containing control cells, suggests that alternative actions of EPI64A in the exocytotic pathway may be enhanced when functional competition with Rab27A is absent. Overall, the data indicate that Rab27A-GTP is critically important in enhancing the size of the IRP and that this is independent of effects on the rate of IRP pool refilling. Rab27A-GTP was also observed integral to setting the overall RRP size, but without substantial effect on pool refilling.

As a test for distinct functional effects between Rab27A and the Rab3 GTPase family we next determined the effects of overexpression of Rab3GAP on IRP and RRP sizes and on pool refilling in pancreatic β-cells. As demonstrated above, Rab3GAP specifically targets the Rab3 isoforms without notable effect on Rab27A-GTP. As shown in Figure 7A,C, overexpression of Rab3GAP in wt β-cells results in an approximately 50% reduction in the IRP from wt control.

By comparison, Rab3GAP overexpression exerted little effect on the RRP when compared with control wt β-cells (Figure 7C). Importantly, the predominate shift in Rab3 isoforms to the GDP-bound state through Rab3GAP overexpression resulted in a substantial deficit in refilling of the IRP and RRP as defined by ΔC_m responses to the subsequent train of step depolarizations (Figure 7A,C). Therefore, it is clear that the GTP-bound state of Rab3 isoforms, but not of Rab27A, are key to rapid refilling of both the IRP and RRP. Although Rab3GAP overexpression reduced integrated Ca^{2+} influx from levels of wt β-cell controls no significant differences were observed on the influx between Rab3GAP-overexpressing control or Ashen cells (Figure 7E), or with EPI64A-overexpressing β-cells (Figure 6C). These data suggest that the specific deficit in pool refilling upon Rab3GAP overexpression is not attributable to reduced Ca^{2+} influx.

To identify potential compensatory functions of Rab27A and Rab3 isoforms in the final stages of exocytosis we next evaluated the effects of combined deficit of Rab27A activity and GTP-bound Rab3 isoforms through overexpression of Rab3GAP in the Ashen β-cells. Ashen cells were used instead of EPI64A co-expression to mitigate alternative actions of EPI64A in the exocytotic pathway. Under these conditions we again observed a reduction in the IRP similar to that seen upon independent reduction of the GTP-bound state of Rab3 isoforms by Rab3GAP overexpression in wt β-cells (Figure 7B,C). Notably, overexpression of Rab3GAP in Ashen cells demonstrated an increased IRP size relative to Ashen alone. This paradoxical result may indicate that enhanced Rab3GAP GTP/GDP cycling of Rab3s may partially offset a Rab27 deficit on the IRP. By comparison, RRP size in the absence of Rab3-GTP and Rab27A was observed to exhibit a substantial and significant reduction greater than that exhibited by Ashen cells or Rab3GAP overexpression alone. In addition, loss of functionally active Rab3-GTP and Rab27A resulted in strongly reduced refilling of the IRP and RRP (Figure 7C). When considered with the findings above, these data demonstrate that GAP overexpression targeting either or both Rab27A or Rab3 proteins reduces IRP size by approximately 50% of wt control. In comparison, individual expression of Rab27A or Rab3 GAP proteins resulted in a smaller effect on the initial size of the RRP, while combined loss of Rab27A and Rab3-GTP isoforms strongly reduced the size of the RRP. A likely interpretation is that Rab27A and Rab3 perform compensatory roles in filling of the IRP and RRP pools. Yet, comparison of the kinetics of refilling of the IRP and RRP pools following depletion indicates that Rab3-GTP isoforms, but not Rab27A, drive rapid refilling of exocytotic SG pools.

Ca^{2+}-triggered insulin secretion from β-cells is potently amplified by increased subplasma membrane cAMP. In addition, the insulinotropic actions of glucagon and incretin hormones are largely mediated via increased cAMP levels, with protein kinase A (PKA) and cAMP-regulated GEF cAMP-GEFII (also termed Epac2) serving as primary downstream cAMP effectors (65–69). Rab3GAP, but not EPI64A, overexpression strongly diminished the rapid refilling of the IRP and RRP following initial depletion. Therefore, we next tested if GTP-bound Rab3 isoforms were required for cAMP to enhance the initial secretory response, and if cAMP signaling was able to offset the Rab3GAP-induced deficit in rapid refilling of the IRP and RRP. For this analysis, the whole-cell recording patch pipettes contained 100 μM cAMP and evaluation of β-cell SG pool parameters of Rab3GAP-overexpressing cells commenced, as above, 90 seconds after attaining the whole-cell configuration. As shown in Figure 8, inclusion of cAMP resulted in a significant increase in initial ΔC_m responses associated with the IRP and RRP compared with Rab3GAP overexpression in wt β-cells. In spite of this cAMP-driven increase in IRP and RRP size, refilling of the pools remained significantly incomplete to the standard 20-second recovery period. Also, although cAMP treatment increased integrated Ca^{2+} influx relative to cells treated with Rab3GAP alone (39.3 ± 6.1 pC, Rab3GAP; 84.1 ± 15.9 pC, Rab3GAP + cAMP) the enhanced influx did not overcome a Rab3GAP-mediated deficit in IRP and RRP pool refilling.

Discussion

The results of this study are among the first to identify and establish unique functional activities of Rab3 and Rab27 proteins on late stages of the exocytotic pathway, while also identifying functional overlap. Notably, we find that establishment of an IRP is completely dependent upon the presence of Rab27A GTPase in β-cells maintained in an islet architecture, as the IRP was completely

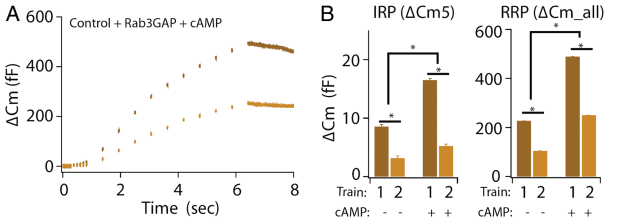

Figure 8: Rab3 actions on rapid refilling of RRP are downstream of cAMP enhancement of IRP and RRP size. A) Averaged ΔC_m to sequentially applied pulse protocols from pAdTrack Rab3GAP/EGFP-infected wt β-cells (brown, $N = 9$ cells, 3 animals) in which the patch pipette solution contained 100 μM cAMP, with darker color showing data from first pulse protocol. B) Averaged size of IRP (left) and RRP (right) for the cAMP recorded pAdTrack Rab3GAP/EGFP-infected wt β-cells. Average results from the non-cAMP Rab3GAP condition (Figure 7) are shown for comparison.

lacking in Ashen β-cells. Rab27A was also found to participate in setting the RRP size under steady-state conditions, as the RRP response to an initial evoked secretory response was significantly reduced in size in Ashen β-cells as well as in wt β-cells overexpressing the Rab27A GAP EPI64A. By comparison, overexpression of Rab3GAP exerted little effect on RRP size under steady-state conditions, although Rab3 GTPases appeared to cooperate with Rab27A in setting the IRP size. Remarkably, however, Rab3, but not Rab27A, GTPases exert a key and prominent role to rapidly refill the IRP and RRP. Assignment of this kinetic effect to Rab3 GTPases resulted from an observed strong deficit in rapid refilling of the RRP upon overexpression of Rab3GAP, and because neither Ashen β-cells nor overexpression of EPI64A in wt β-cells demonstrated a kinetic deficit in IRP and RRP refilling. Interestingly, the kinetic deficit in Rab3GAP-overexpressing β-cells did not mitigate cAMP from strongly potentiating the steady-state IRP and RRP size, although notably, refilling of these pools following depletion remained incomplete. Our experimental conditions do not exclude the possibility that the Rab3GAP-mediated slowing of refilling is independent of Rab3. However, previous studies have demonstrated that loss of Rab3GAP results in no changes in the levels of key exocytotic proteins or morphology of release sites (70,71). Moreover, Müller et al. showed that Rab3 specifically mediated a deficit in compensatory synaptic exocytosis in Rab3GAP mutant synapses. Taken together, these data support that Rab3GAP actions on secretion being directly related to perturbations in the activity of Rab3 GTPases. Finally, the combined loss of active Rab3 GTPases with Rab27A resulted in an RRP size that was more severely reduced than observed in Ashen β-cells. Notably, the present results complement our initial report that established incomplete refilling of the RRP following its evoked depletion in isolated and cultured Ashen β-cells (13). In addition, we reported that β-cells lacking only the Rab3A isoform displayed normal IRP and RRP refilling, which together with the present results suggest that other Rab3 isoforms are able to fully compensate for loss of Rab3A. The present data demonstrate distinct functional and kinetic regulatory activities of Rab3 and Rab27A GTPases on SG transition to fusion competency, while also providing evidence that full development of β-cell secretory activity requires convergent actions of Rab3 and Rab27A GTPases.

An important feature of this study is that we have identified unique roles for Rab27 and Rab3 GTPases. Rab27 GTPases are necessary for the formation of an IRP. This was a surprising result given the extensive literature linking Rab3/RIM complexes with docking near calcium channels, as required for the IRP (19,72–74). Nonetheless, our results suggest that Rab27 is a limiting factor for the formation of the IRP, which could be mediated by Rab27 unfettering of Rab3-clamped granules through stimulation of GTPase activity (75), or via Rab27 complexes with Slp4A/Munc18-1/Syntaxin (76). Rab3A GTPases exert a unique role on the rapid repopulation of the IRP and RRP in pancreatic β-cells. Yet, the mechanism by which Rab3 GTPases exert this action remains unanswered. Biochemical, genetic and live cell imaging have demonstrated that targeting/docking and priming functions of Rab GTPases involve a sequencing of effector interactions (77). In addition, multiple lines of evidence have indicated that docked SGs may be the primary location of Rab3 GTPase priming actions, because Rab3GAP hydrolyzes Rab3-GTP to Rab3-GDP concurrently with Ca^{2+}-triggered vesicle fusion (77–79). This catalytic event is believed to occur after vesicle docking/tethering but prior to endocytosis, as Rab3 is absent from clathrin-containing vesicles (80). Rab effectors interact directly, or in molecular scaffolds, with other mediators of vesicle priming and membrane fusion. For example, Rab3 GTPase effectors include rabphilin

(17), Noc2 (39), Slp4 (35), Munc18-1 (81) and RIM1α/2α (18). Notably, RIM1α/2α bind with the priming factor Munc13-1 and nuclear magnetic resonance spectroscopy has established that Rab3-GTP, Rim2α and Munc13-1 can assemble into a tripartite complex (82). RIM has been established to exert a key role in insulin secretion (83) and be associated with both Rab3-GTP on the insulin granule (19) and L-type Ca^{2+} channels on the plasma membrane (84). In addition to effector interaction with RIM, Rab3-GTP interactions with Munc18-1 or rabphilin may serve as the link between granule docking and priming reactions with SNARE proteins (81,85). These results have led to a model whereby a secretory stimulus enhances GTP hydrolysis to elicit disassembly of the GTP-bound Rab–effector complexes, thereby allowing the spatially localized interaction of Rab effectors with downstream mediators required for vesicle priming/fusion and formation of the SNARE complex (77, 78, 86, 87). Moreover, recent reconstitution of Rab5 with its cognate SNARE-dependent membrane fusion pathway has demonstrated that Rab and SNARE machineries act coordinately to facilitate the process of membrane tethering/docking and fusion (88). Importantly, although Rab3 GTPases may serve as gatekeepers regulating transition of docked SGs into primed releasable pools, the specific SGs on which Rab3 acts to rapidly refill the RRP remain unknown, particularly as insulin SGs are subject to rapid recruitment and priming during sustained glucose-stimulated insulin secretion (89,90).

Glucose-stimulated β-cell secretion is biphasic, consisting of a rapid and a slower more prolonged phase of insulin release. The initial phase has generally been equated with the IRP, which is completely released over milliseconds in response to step depolarization under voltage clamp (91). This association is based on the number of SGs released, and on timing differences between the direct electrical- and glucose-evoked release resulting from the immediacy of membrane potential changes versus glucose diffusion, uptake and metabolism and insulin diffusion from an intact tissue. In addition, molecular scaffolding of a small set of SGs to voltage-gated calcium channels, and of insensitivity of fusion of the IRP by the Ca^{2+} chelator EGTA, but not the kinetically faster chelator BAPTA, have strongly indicated that the IRP consists of docked SGs. Moreover, TIRF imaging of insulin SGs has demonstrated that the initial rapid fusion events result largely from membrane adjacent/docked SGs (92–94). Taken together, release from the IRP is likely to be completely accounted for by fusion of membrane-docked SGs.

By comparison, the source of SGs that comprise the RRP (generally assigned to the second phase of glucose-stimulated insulin secretion) is less concretely identified. This pool likely is composed of docked (or membrane resident) SGs as well as a set of newcomer granules that have more recently been identified to cycle rapidly from the RP to undergo membrane fusion (95). Previous findings have established that Rab3 and Rab27 GTPases coordinately regulate the docking of dense core SGs (46) while also differing in membrane cycling dynamics (32). Our data demonstrate that the formation of an IRP is completely dependent upon Rab27A, with active Rab3 GTPases exerting a modulatory role. For the RRP, active Rab3 GTPases exert a critical role on rapid refilling of the RRP following initial depletion, while GTP-bound Rab27A appears important in defining the overall size of the RRP. Thus, although overexpression of Rab3GAP slowed RRP refilling it did not notably affect RRP size. The divergent actions of these Rab GTPases may correlate with differences reported in their dynamic association with SGs (32,33,96). The Rab3A pool, which likely reflects similar behavior of the other Rab3 GTPases, demonstrates a rapid exchange between the SGs and cytosol, whereas Rab27A has demonstrated little exchange associated with the exocytotic event (32,33). The rapid exchange of Rab3 GTPases may account for their ability to kinetically facilitate RRP refilling as they are able to quickly cycle onto SGs and recruit appropriate effectors that promote SG recruitment to the plasma membrane as well as subsequent tethering/docking and priming processes. Not only is rapid granule/cytosolic exchange lacking for Rab27A, fluorescence recovery after photobleaching studies have indicated that once it associates with newly synthesized SGs it becomes non-exchangeable, perhaps as a result of low inherent GTPase activity (32). In support of its low GTPase activity, a high percentage of Rab27A has been reported to be GTP-bound and membrane-associated, even in unstimulated pituitary, platelet, pancreatic acinar and insulin-secreting Min6 cells (20,97,98). Yet, GTPase activity appears key to regulation of insulin secretion because Rab27A, unlike most GTPases, has been reported

to bind effectors in both the GDP- and GTP-bound states. In its GDP-bound state, Rab27A recruits and interacts with Slp4A (37). Slp4A (also termed granuphilin) was originally identified in pancreatic β-cells as a protein that binds to the closed form of syntaxin1A and Rab27A-GDP to participate in docking of the insulin granules (20,99,100). Yet, this Rab27A-GDP-directed docking complex has been reported to be extremely stable and strongly inhibitory to the progression of SG priming and membrane fusion (35,101). Release of this clamp on granule priming is believed to require the transition of Rab27A to its GTP-bound state, although Rab27A-GTP retains high-affinity Slp4A binding. Interestingly, the Rab27A/granuphilin/syntaxin1A complex may also contain Munc18 (99), an apparent regulator with Munc13 of SNARE complex assembly, suggesting that transition of Rab27A from GDP- to GTP-bound state may also allow initiation of priming processes. Our data demonstrating a reduction in RRP size in Ashen β-cells are consistent with Rab27A promoting stability of SG tethering/docking and priming into the RRP. In addition, complete elimination of the IRP in Ashen β-cells suggests that Rab27A may also be important in targeting insulin SGs to membrane nanodomains adjacent to voltage-gated calcium channels.

While glucose stimulation of β-cells may facilitate transition of Rab27A from its GDP- to GTP-bound state and promote vesicle priming, it also drives Rab3-GTP binding (75), vesicle fusion and a coincident cycling of Rab27A back to a GDP-bound state. Unlike Rab3 GTPases, post-fusion membrane-associated Rab27-GDP in pancreatic β-cells does not rapidly exchange into the cytosol, but rather acts to recruit and activate the endocytotic regulators coronin3 and Cdc42-GTP-bound IQGAP1 (34,102). The interaction of Rab27A-GDP with coronin3, a promoter of F-actin bundling, in complex with IQGAP1 has been reported essential for endocytosis of insulin secretory membrane. Moreover, overexpression of EPI64A in β-cells has previously been found to reproduce glucose-dependent translocation of coronin3 (103), likely resulting from GTP hydrolysis and production of Rab27A-GDP. The negative clamp on exocytotic activity of Rab27A-GDP through Slp4A interaction, and its slow exchange into the cytosol following exocytosis may account for its kinetically slower action on refilling of the vesicle pools from newcomer granules than that of Rab3.

It is important to note that while we have identified distinct functional activities of Rab3 and Rab27 GTPases in the exocytotic pathway, these GTPases also demonstrated a high degree of functional commonality. For example, the RRP, while reduced in Ashen β-cells as well as in wt β-cells overexpressing EPI64A, remained present and rapidly refilled following the depolarization-evoked depletion protocol. Rab3 GTPases also largely compensated for Rab27 absence, as evidenced by an even stronger reduction in RRP size and pool refilling upon Rab3GAP overexpression in Ashen β-cells. Conversely, Rab27A also appears to exert substantial functional compensation when Rab3 GTPases are shifted to their GDP-bound state by Rab3GAP overexpression, as there was little effect on RRP size, although the rate of refilling was significantly slowed. This functional overlap is likely based on the high homology between Rab3 and Rab27 (57% by amino acid sequence) that leads to sharing of a number of effectors (rabphilin, Noc2 and Slp4A). Also, even where Rab3 and Rab27A exhibit effector selectivity (Rab3, RIM1/2a, Rab27A, Slac2-C and Munc13-4) the effectors demonstrate overlap in their reported functional activities (19,21,40).

In summary, our data are novel in identifying unique functional activities of Rab3 and Rab27 GTPases within the exocytotic pathway. Identification of the precise pathways that govern these mechanistic differences requires further investigation. Our data further suggest that Rab3 GTPases act to rapidly refill releasable granule pools but that Rab27 may demarcate and define the quantity of releasable sites as well as be required to populate the IRP. The linear sequencing of SGs from the RRP to IRP suggests a dynamic coordination in GTPase activity and/or effector switching during secretagogue stimulation. In addition, while functional diversity is distinguishable, there remain considerable compensatory actions between these GTPases, which likely result from the cooperative use of effectors and/or specificity in effectors with functional similarity. Future investigations require evaluating whether all the isoforms of Rab3 participate in rapid refilling of the RRP and identifying which most effectively compensates for loss of Rab27A.

Materials and Methods

Mice and pancreatic islet slice preparation

All experiments were approved by the University Committee on Use and Care of Animals (UCUCA) and appropriate measures were taken to reduce the pain of experimental animals. Mice carrying a spontaneous A to T transversion mutation in the Rab27A gene (ash/ash; C3H/He background) lead to the production of a non-functional Rab27A protein that lacks critical domains of the GTP-binding pocket. These Ashen mice were initially supplied by N. A. Jenkins (National Cancer Institute) in cooperation with Jackson Laboratories. Gender- and age-matched mice of the same background strain variant (C3H/HeSnJ) were used as controls. Mice were sacrificed by CO_2 asphyxiation, decapitated and the pancreas sterilely removed for preparation of isolated islets. Collagenase P (1 mg/mL, Roche Diagnostics), soybean trypsin inhibitor (0.1 mg/mL) and neutralized bovine serum albumin (2.5 mg/mL) dissolved in 5 mL of 5% CO_2/95% O_2 gassed F12K Nutrient Kaighn's media were immediately injected into the pancreas until well distended. Following injection, the pancreas and remaining collagenase solution were placed in a 25-mL Erlenmeyer flask, gassed with 5% CO_2/95% O_2 and placed into a 37°C oscillating water bath (100 cycles/min) for 10 min. Following this period, free collagenase solution surrounding the pancreas was removed and replaced with a fresh 5-mL aliquot of collagenase solution and the flask returned to the oscillating water bath for an additional 15 min. Dispersion of the pancreas to generate isolated islets and acini was then performed by sequential passage through polypropylene pipettes of decreasing tip diameter. The resulting cell suspension was transferred to a 10-cm culture plate and individual intact islets identified using an inverted microscope were removed by hand micropipetting into a F12K media-containing collection dish. The isolated islets were then collected and placed into 37°C liquid agarose (low melting point) and centrifuged at 1700 × ***g*** at 25°C for 2 min. Horizontal slices (150 μm) were then cut from the islets concentrated at the tip of the solidified agarose and transferred to millicell-supported membranes (0.4 μm pore; Millipore, Cork IRL) in culture media (DMEM, 15% heat-inactivated FBS, 0.0005% β-mercaptoethanol, 50 U/mL penicillin, 50 μg/mL streptomycin and 0.05 mg/mL soybean trypsin inhibitor) for 1–3 days of organ culture.

Expression constructs and viral infection

Expression of exogenously introduced transgenes in cells of cultured islets was accomplished using adenoviral infection. The vector pAdTrack-CMV (Addgene) was used for subcloning into and for infection and expression of the catalytic subunit of Rab3GAP (Yoshimi Takai, Kobe University), EPI64A (Open Biosystems, Thermo Scientific) or β-Gal (control). The sequence fidelity of all constructs was confirmed by DNA sequencing (University of Michigan DNA Sequencing Core). Islets were infected with viral aliquots sufficient to infect approximately 20% of the surface layer of cells within a slice. Virus was diluted in media and applied directly onto the islets and into the small volume of media resident on the millicell membrane surface. After 12 h the media were exchanged for fresh culture media. To identify infected cells the pAdTrack contained an independent CMV promoter driving expression of the fluorescent EGFP tracer.

Islet slice electrophysiology

Islet slices surrounded by the agarose matrix were transferred to a continuously perfused and temperature-controlled (31°C) recording chamber (Warner Instruments) that was mounted on an upright Nikon EF-89 microscope and equipped with a 40× water immersion lens (NA 1.2) for viewing of individual cells. Whole-cell patch-clamp experiments were performed on cells within islet slices using an EPC-9 or EPC-10 amplifier and PATCHMASTER acquisition software (HEKA Elektronik). Patch pipettes with a resistance of 3–6 MΩ when filled with the pipette solution were pulled from Schott capillary glass containing a microfiber (AM Systems) and then coated with Sylgard (Dow Corning) to reduce capacitance transients. Currents underlying test pulses and $I-V$ relationships were compensated for linear leak current using a P/4 protocol.

Evoked changes in cell capacitance associated with exocytotic activity were measured using the PATCHMASTER software lock-in extension (sine + DC) with a 30-mV peak sinusoid signal applied at a frequency of 1.8 kHz. Data were analyzed only if the resulting Rs maintained <20 MΩ. Although β-cells are electrically coupled, previous reports have established that only 1.5% of the current response to the sine wave originates from neighboring cells (104). In addition, although changes in membrane capacitance reflect a net measurement of exocytotic and endocytotic activity, endocytosis operates at a significantly slower rate than exocytosis, suggesting that the rapid sequential voltage-step-evoked responses largely represent exocytotic activity. The standard extracellular solution contained (mM): 135 NaCl, 2.5 KCl, 1.25 NaH_2PO_4, 2 sodium pyruvate, 0.5 ascorbic acid, 1 $MgCl_2$, 2 $CaCl_2$, 3 glucose and 26 $NaHCO_3$. The solution was gassed continuously with 5% CO_2/95% O_2 for a pH of 7.4. In experiments where glucose concentration was raised the NaCl was reduced to maintain an equivalent osmolality (290 mOsmol/L). The pipette solution used for whole-cell recording contained (mM): 120 Cs-glutamate, 10 NaCl, 10 KCl, 1 $MgCl_2$, 10 HEPES (pH 7.15 with CsOH), 0.05 EGTA, 3 Mg-ATP and 0.2 Na-GTP. Current-clamp recordings from β-cells in islet slices were performed using amphotericin (250 μg/mL)-perforated patch-clamp conditions with the following pipette solution (mM): 76 K_2SO_4, 5 NaCl, 10 KCl, 1 $MgCl_2$, 0.2 EGTA and 10 HEPES (pH 7.35 with KOH). All reagents were from Sigma unless stated otherwise.

Confocal microscopy

Confocal imaging was performed on an Olympus IX81 disc-spinning confocal microscope using a Plan-Apochromat 100× oil immersion objective (1.4 NA). Fluorescent illumination was provided by a Lambda LS 300-W xenon arc lamp (Sutter Instruments) coupled to a shuttered liquid light guide for controlled transmission of light to the microscope optics. Images were acquired using an electron multiplying charge-coupled device (EM-CCD) Hamamatsu (ImagEM) camera and a 2× optical zoom (Optem). Monomeric versions of mCH, YFP, Citrine (a YFP derivative of reduced pH sensitivity), CFP, Cerulean or EGFP N-terminal fluoroprotein-tagged fusion proteins were imaged using the following excitation/emission filter sets: Ex 472/30; 562/40; 501/18; 416/25 and Em: 520/35; 641/75; 547/31; 464/23, respectively. Prior to image acquisition the illumination intensity/camera gain of each fluorescence channel was optimized to ensure a full dynamic range (16-bit

image). Once acquisition parameters were determined, identical settings were used for each condition being compared. Cytofluorograms for Rab GTPases versus granules (NPY-mCH), see Figure 2B, were constructed by taking background-subtracted (rolling-ball radius filter = 100 pixels) intensities of each pixel per channel and plotting them against one another. A Pearson's r correlation coefficient was then calculated to indicate the degree of colocalization between Rabs and granules.

Total internal reflection fluorescence microscopy

TIRF imaging of SG mobility in transfected MIN6 cells was performed on an Olympus IX71 microscope equipped with a 60× oil immersion objective (1.49 NA). Cells were co-transfected with Citrine (control) or a N-terminal Citrine-tagged Rab3GAP and/or EPI64A along with NPY-mCH to label the lumen of insulin-containing SGs. TIRF imaging of MIN6 cells was performed in a physiological saline containing (mM): 135 NaCl, 5 KCl, 1 $MgCl_2$, 2 $CaCl_2$, 3 glucose and 10 HEPES (pH 7.4). For illumination, two lasers including a 50-mW diode-pumped solid-state laser operating at a fixed wavelength of 594 nm (Cobolt Mambo) and a 225-mW Argon-ion laser (National Laser Company) beam (selected 488-nm laser line) were passed through a acousto-optic tunable filter (AOTF) to select the passing laser line and adjust illumination power. Output of the AOTF was coupled to a unimodal fiber optic that was directed through beam expansion optics immediately prior to being reflected into the microscope body by a mirror mounted on a galvanometer to position the laser illumination in the back focal plane of the objective. The position of the 488-nm laser line in the back focal plane was adjusted to set a resulting evanescent field depth of 100 nm. An additional achromatic lens between the mirror and the microscope objective focused the laser on the back focal plane of the objective. The microscopes filter cube assembly contains a laser clean-up filter (488 ± 10 nm), dichroic mirror (z488rdc) and emitter (HQ525/50). All filters were laser grade from Chroma Technologies. Fluorescence emission images were acquired with a 16-bit, 512 × 512 pixel Photometrics QuantEM 512SC EM-CCD camera (Roper Scientific) with 16 × 16 μm pixel size. To achieve Nyquist sampling, emission was submitted to additional magnification from a 1.6× magnifier on the IX71 and a 2.5× beam expander. The laser lines, laser powers, incident angle and camera were controlled using METAMORPH software (Molecular Devices).

Images were acquired at 20 Hz and with mobility in x–y and axial (z) dimensions determined by tracking granules that were present throughout the entire image series in each cell using custom-written MATLAB scripts. Granule detection was accomplished by applying a binary mask to each image, with the default masking threshold set to 15 standard deviations above the mean of a background region of interest. The centroid coordinates of each granule in each masked image were determined and a comparison of granule centroids across frames was used to identify those SGs that remained throughout the complete image series. Each of these SGs was then individually tracked by applying a 2D Gaussian fit for the granule in its first frame, and then searching a 12 × 12 pixel region surrounding the granule's fitted center coordinates in the next frame, for a similar Gaussian fit. Specific limits were set for acceptable changes in x–y position and minimum time spent at a position for a given granule to be considered the same. Granule tracking was terminated if two unique granules collided. Changes in x–y position between frames for each granule were determined using its center coordinates. For axial motion, fluorescence intensity for each tracked granule per frame was determined using a granule's center coordinates to center a 3 × 3 pixel mask and measure averaged intensity. The apparent interframe fluctuations in central x–y positions $(\Delta R)^2$ and fluorescence intensity $(\Delta Z')^2$ were determined as previously described (105), with apparent integrated intensity fluctuations occurring between frames for individual granules $(\Delta Z')^2$ corrected for instrumental noise (shot noise and EM-CCD camera noise) by imaging tetraspeck beads adhered to a glass coverslip to generate corrected $(\Delta Z)^2$. Interframe x–y mobility represented by $(\Delta R)^2$ was calculated by: $(\Delta R)^2 = ((x_2 - x_1)^2 + (y_2 - y_1)^2)$*83.3 nm/pixel, where x and y represent the centroid position between paired interframe intervals 1 and 2. Apparent interframe axial mobility $(\Delta Z')^2$ is based on background-subtracted intensities (I) in successive frames (1 and 2) and with $z = 0$ defined as the brightest intensity granule (I_o) per cell. Characteristic TIRF depth (Dp) was set at 100 nm. For each frame (i) the apparent intensity (I'_i) is calculated as: $I'_i = I_o e^{-z'i/Dp}$, which upon rearranging results in: $z'_i = -Dp\ \ln\left(I'_i/I_o\right)$.

Statistics

All statistical analysis was done using GraphPad Prism. Where indicated, one-way analysis of variance (ANOVA) was used to test for significant differences (significance was set to a $p < 0.05$). *Post hoc* Bonferroni protected t-tests were used for comparisons between specific groups. To test whether cumulative frequency distributions of granule mobility were significantly different, we employed the Kolmogorov–Smirnov test. Statistical significance at a $p < 0.05$ is noted within figures by an asterisk (*).

Acknowledgments

This work was supported by NIH grant RO1 NIDDK-DK077050 to E. L. S. We thank Dr. Yanan Hou for critical discussions related to the experiments and specific research reagents.

References

1. Porte D, Kahn SE. Beta-cell dysfunction and failure in type 2 diabetes: potential mechanisms. Diabetes 2001;50(Suppl 1): S160–S163.
2. Ashcroft FM, Rorsman P. KATP channels and islet hormone secretion: new insights and controversies. Nat Rev Endocrinol 2013;9:660–669.
3. Henquin JC. Triggering and amplifying pathways of regulation of insulin secretion by glucose. Diabetes 2000;49:1751–1760.
4. Straub SG, Sharp GWG. Glucose-stimulated signaling pathways in biphasic insulin secretion. Diabetes Metab Res Rev 2002;18:451–463.

5. Rutter GA. Visualising insulin secretion. The Minkowski Lecture 2004. Diabetologia 2004;47:1861–1872.
6. MacDonald PE, Joseph JW, Rorsman P. Glucose-sensing mechanisms in pancreatic beta-cells. Philos Trans R Soc Lond B Biol Sci 2005;360:2211–2225.
7. Sadoul K, Lang J, Montecucco C, Weller U, Regazzi R, Catsicas S, Wollheim CB, Halban PA. SNAP-25 is expressed in islets of Langerhans and is involved in insulin release. J Cell Biol 1995;128:1019–1028.
8. Nagamatsu S, Fujiwara T, Nakamichi Y, Watanabe T, Katahira H, Sawa H, Akagawa K. Expression and functional role of syntaxin 1/HPC-1 in pancreatic beta cells. Syntaxin 1A, but not 1B, plays a negative role in regulatory insulin release pathway. J Biol Chem 1996;271:1160–1165.
9. Gaisano HY, Ostenson C-G, Sheu L, Wheeler MB, Efendic S. Abnormal expression of pancreatic islet exocytotic soluble N-ethylmaleimide-sensitive factor attachment protein receptors in Goto-Kakizaki rats is partially restored by phlorizin treatment and accentuated by high glucose treatment. Endocrinology 2002;143:4218–4226.
10. Zerial M, McBride H. Rab proteins as membrane organizers. Nat Rev Mol Cell Biol 2001;2:107–117.
11. Hutagalung AH, Novick PJ. Role of Rab GTPases in membrane traffic and cell physiology. Physiol Rev 2011;91:119–149.
12. Regazzi R, Vallar L, Ullrich S, Ravazzola M, Kikuchi A, Takai Y, Wollheim CB. Characterization of small-molecular-mass guanine-nucleotide-binding regulatory proteins in insulin-secreting cells and PC12 cells. Eur J Biochem 1992;208:729–737.
13. Merrins MJ, Stuenkel EL. Kinetics of Rab27a-dependent actions on vesicle docking and priming in pancreatic beta-cells. J Physiol (Lond) 2008;586:5367–5381.
14. Schlüter OM, Schmitz F, Jahn R, Rosenmund C, Südhof TC. A complete genetic analysis of neuronal Rab3 function. J Neurosci 2004;24:6629–6637.
15. Regazzi R, Ravazzola M, Iezzi M, Lang J, Zahraoui A, Andereggen E, Morel P, Takai Y, Wollheim CB. Expression, localization and functional role of small GTPases of the Rab3 family in insulin-secreting cells. J Cell Sci 1996;109:2265–2273.
16. Coppola T, Perret-Menoud V, Lüthi S, Farnsworth CC, Glomset JA, Regazzi R. Disruption of Rab3-calmodulin interaction, but not other effector interactions, prevents Rab3 inhibition of exocytosis. EMBO J 1999;18:5885–5891.
17. Chung SH, Joberty G, Gelino EA, Macara IG, Holz RW. Comparison of the effects on secretion in chromaffin and PC12 cells of Rab3 family members and mutants. Evidence that inhibitory effects are independent of direct interaction with Rabphilin3. J Biol Chem 1999;274:18113–18120.
18. Fukuda M. Assay and functional interactions of Rim2 with Rab3. Methods Enzymol 2005;403:457–468.
19. Yasuda T, Shibasaki T, Minami K, Takahashi H, Mizoguchi A, Uriu Y, Numata T, Mori Y, Miyazaki J-I, Miki T, Seino S. Rim2a determines docking and priming states in insulin granule exocytosis. Cell Metab 2010;12:117–129.
20. Zhao S, Torii S, Yokota-Hashimoto H, Takeuchi T, Izumi T. Involvement of Rab27b in the regulated secretion of pituitary hormones. Endocrinology 2002;143:1817–1824.
21. Waselle L, Coppola T, Fukuda M, Iezzi M, El-Amraoui A, Petit C, Regazzi R. Involvement of the Rab27 binding protein Slac2c/MyRIP in insulin exocytosis. Mol Biol Cell 2003;14:4103–4113.
22. Lam AD, Ismail S, Wu R, Yizhar O, Passmore DR, Ernst SA, Stuenkel EL. Mapping dynamic protein interactions to insulin secretory granule behavior with TIRF-FRET. Biophys J 2010;99:1311–1320.
23. Haddad EK, Wu X, Hammer JA, Henkart PA. Defective granule exocytosis in Rab27a-deficient lymphocytes from Ashen mice. J Cell Biol 2001;152:835–842.
24. Kasai K, Ohara-Imaizumi M, Takahashi N, Mizutani S, Zhao S, Kikuta T, Kasai H, Nagamatsu S, Gomi H, Izumi T. Rab27a mediates the tight docking of insulin granules onto the plasma membrane during glucose stimulation. J Clin Invest 2005;115:388–396.
25. Yi Z, Yokota H, Torii S, Aoki T, Hosaka M, Zhao S, Takata K, Takeuchi T, Izumi T. The Rab27a/granuphilin complex regulates the exocytosis of insulin-containing dense-core granules. Mol Cell Biol 2002;22:1858–1867.
26. Pavlos NJ, Jahn R. Distinct yet overlapping roles of Rab GTPases on synaptic vesicles. Small GTPases 2011;2:77–81.
27. Iezzi M, Escher G, Meda P, Charollais A, Baldini G, Darchen F, Wollheim CB, Regazzi R. Subcellular distribution and function of Rab3A, B, C, and D isoforms in insulin-secreting cells. Mol Endocrinol 1999;13:202–212.
28. Barr F, Lambright DG. Rab GEFs and GAPs. Curr Opin Cell Biol 2010;22:461–470.
29. Figueiredo AC, Wasmeier C, Tarafder AK, Ramalho JS, Baron RA, Seabra MC. Rab3GEP is the non-redundant guanine nucleotide exchange factor for Rab27a in melanocytes. J Biol Chem 2008;283:23209–23216.
30. Tanaka M, Miyoshi J, Ishizaki H, Togawa A, Ohnishi K, Endo K, Matsubara K, Mizoguchi A, Nagano T, Sato M, Sasaki T, Takai Y. Role of Rab3 GDP/GTP exchange protein in synaptic vesicle trafficking at the mouse neuromuscular junction. Mol Biol Cell 2001;12:1421–1430.
31. Itoh T, Fukuda M. Identification of EPI64 as a GTPase-activating protein specific for Rab27A. J Biol Chem 2006;281:31823–31831.
32. Handley MTW, Haynes LP, Burgoyne RD. Differential dynamics of Rab3A and Rab27A on secretory granules. J Cell Sci 2007;120:973–984.
33. Pavlos NJ, Grønborg M, Riedel D, Chua JJE, Boyken J, Kloepper TH, Urlaub H, Rizzoli SO, Jahn R. Quantitative analysis of synaptic vesicle Rabs uncovers distinct yet overlapping roles for Rab3a and Rab27b in Ca^{2+}-triggered exocytosis. J Neurosci 2010;30:13441–13453.
34. Kimura T, Kaneko Y, Yamada S, Ishihara H, Senda T, Iwamatsu A, Niki I. The GDP-dependent Rab27a effector coronin 3 controls endocytosis of secretory membrane in insulin-secreting cell lines. J Cell Sci 2008;121:3092–3098.
35. Fukuda M. Slp4-a/granuphilin-a inhibits dense-core vesicle exocytosis through interaction with the GDP-bound form of Rab27A in PC12 cells. J Biol Chem 2003;278:15390–15396.

36. Kondo H, Shirakawa R, Higashi T, Kawato M, Fukuda M, Kita T, Horiuchi H. Constitutive GDP/GTP exchange and secretion-dependent GTP hydrolysis activity for Rab27 in platelets. J Biol Chem 2006;281:28657–28665.
37. Fukuda M. Rab27 and its effectors in secretory granule exocytosis: a novel docking machinery composed of a Rab27.effector complex. Biochem Soc Trans 2006;34:691–695.
38. Fukuda M. Distinct Rab binding specificity of Rim1, Rim2, rabphilin, and Noc2. Identification of a critical determinant of Rab3A/Rab27A recognition by Rim2. J Biol Chem 2003;278:15373–15380.
39. Cheviet S, Waselle L, Regazzi R. Noc-king out exocrine and endocrine secretion. Trends Cell Biol 2004;14:525–528.
40. Shirakawa R. Munc13-4 is a GTP-Rab27-binding protein regulating dense core granule secretion in platelets. J Biol Chem 2003;279:10730–10737.
41. Handley MTW, Burgoyne RD. The Rab27 effector Rabphilin, unlike Granuphilin and Noc2, rapidly exchanges between secretory granules and cytosol in PC12 cells. Biochem Biophys Res Commun 2008;373:275–281.
42. Göpel S, Kanno T, Barg S, Galvanovskis J, Rorsman P. Voltage-gated and resting membrane currents recorded from B-cells in intact mouse pancreatic islets. J Physiol (Lond) 1999;521:717–728.
43. Huang Y-C, Rupnik M, Gaisano HY. Unperturbed islet α-cell function examined in mouse pancreas tissue slices. J Physiol (Lond) 2011;589:395–408.
44. Fukui K, Sasaki T, Imazumi K, Matsuura Y, Nakanishi H, Takai Y. Isolation and characterization of a GTPase activating protein specific for the Rab3 subfamily of small G proteins. J Biol Chem 1997;272:4655–4658.
45. Grosshans BL, Andreeva A, Gangar A, Niessen S, Yates JR, Brennwald P, Novick P. The yeast lgl family member Sro7p is an effector of the secretory Rab GTPase Sec4p. J Cell Biol 2006;172:55–66.
46. Tsuboi T, Fukuda M. Rab3A and Rab27A cooperatively regulate the docking step of dense-core vesicle exocytosis in PC12 cells. J Cell Sci 2006;119:2196–2203.
47. Stevens DR, Schirra C, Becherer U, Rettig J. Vesicle pools: lessons from adrenal chromaffin cells. Front Synaptic Neurosci 2011;3:2.
48. Feng W, Liang T, Yu J, Zhou W, Zhang Y, Wu Z, Xu T. RAB-27 and its effector RBF-1 regulate the tethering and docking steps of DCV exocytosis in *C. elegans*. Sci China Life Sci 2012;55:228–235.
49. Leenders AG, Lopes da Silva FH, Ghijsen WE, Verhage M. Rab3a is involved in transport of synaptic vesicles to the active zone in mouse brain nerve terminals. Mol Biol Cell 2001;12:3095–3102.
50. Coleman WL, Bill CA, Bykhovskaia M. Rab3a deletion reduces vesicle docking and transmitter release at the mouse diaphragm synapse. Neuroscience 2007;148:1–6.
51. Gomi H, Mori K, Itohara S, Izumi T. Rab27b is expressed in a wide range of exocytic cells and involved in the delivery of secretory granules near the plasma membrane. Mol Biol Cell 2007;18:4377–4386.
52. Johnson JL, Brzezinska AA, Tolmachova T, Munafo DB, Ellis BA, Seabra MC, Hong H, Catz SD. Rab27a and Rab27b regulate neutrophil azurophilic granule exocytosis and NADPH oxidase activity by independent mechanisms. Traffic 2010;11:533–547.
53. Burke NV, Han W, Li D, Takimoto K, Watkins SC, Levitan ES. Neuronal peptide release is limited by secretory granule mobility. Neuron 1997;19:1095–1102.
54. Oheim M, Loerke D, Stühmer W, Chow RH. The last few milliseconds in the life of a secretory granule. Docking, dynamics and fusion visualized by total internal reflection fluorescence microscopy (TIRFM). Eur Biophys J 1998;27:83–98.
55. Steyer JA, Almers W. Tracking single secretory granules in live chromaffin cells by evanescent-field fluorescence microscopy. Biophys J 1999;76:2262.
56. Johns LM. Restriction of secretory granule motion near the plasma membrane of chromaffin cells. J Cell Biol 2001;153:177–190.
57. Degtyar VE, Allersma MW, Axelrod D, Holz RW. Increased motion and travel, rather than stable docking, characterize the last moments before secretory granule fusion. Proc Natl Acad Sci U S A 2007;104:15929–15934.
58. Straub SG, Shanmugam G, Sharp GWG. Stimulation of insulin release by glucose is associated with an increase in the number of docked granules in the beta-cells of rat pancreatic islets. Diabetes 2004;53:3179–3183.
59. Barg S, Eliasson L, Renström E, Rorsman P. A subset of 50 secretory granules in close contact with L-type Ca^{2+} channels accounts for first-phase insulin secretion in mouse beta-cells. Diabetes 2002;51(Suppl 1):S74–S82.
60. Olofsson CS, Göpel SO, Barg S, Galvanovskis J, Ma X, Salehi A, Rorsman P, Eliasson L. Fast insulin secretion reflects exocytosis of docked granules in mouse pancreatic B-cells. Pflugers Arch 2002;444:43–51.
61. Ge Q, Dong Y-M, Hu Z-T, Wu Z-X, Xu T. Characteristics of Ca^{2+}-exocytosis coupling in isolated mouse pancreatic beta cells. Acta Pharmacol Sin 2006;27:933–938.
62. Yang Y, Gillis KD. A highly Ca^{2+}-sensitive pool of granules is regulated by glucose and protein kinases in insulin-secreting INS-1 cells. J Gen Physiol 2004;124:641–651.
63. Regazzi R, Kikuchi A, Takai Y, Wollheim CB. The small GTP-binding proteins in the cytosol of insulin-secreting cells are complexed to GDP dissociation inhibitor proteins. J Biol Chem 1992;267:17512–17519.
64. Reczek D. Identification of EPI64, a TBC/rabGAP domain-containing microvillar protein that binds to the first PDZ domain of EBP50 and E3KARP. J Cell Biol 2001;153:191–206.
65. Malaisse WJ, Malaisse-Lagae F, Mayhew D. A possible role for the adenylcyclase system in insulin secretion. J Clin Invest 1967;46:1724–1734.
66. Montague W, Howell SL. The mode of action of adenosine 3′:5′-cyclic monophosphate in mammalian islets of Langerhans. Preparation and properties of islet-cell protein phosphokinase. Biochem J 1972;129:551–560.
67. Pipeleers DG, in't Veld PA, Van de Winkel M, Maes E, Schuit FC, Gepts W. A new in vitro model for the study of pancreatic A and B cells. Endocrinology 1985;117:806–816.

68. Kashima Y, Miki T, Shibasaki T, Ozaki N, Miyazaki M, Yano H, Seino S. Critical role of cAMP-GEFII--Rim2 complex in incretin-potentiated insulin secretion. J Biol Chem 2001;276:46046–46053.
69. Shibasaki T, Sunaga Y, Fujimoto K, Kashima Y, Seino S. Interaction of ATP sensor, cAMP sensor, Ca^{2+} sensor, and voltage-dependent Ca^{2+} channel in insulin granule exocytosis. J Biol Chem 2004;279:7956–7961.
70. Sakane A, Manabe S, Ishizaki H, Tanaka-Okamoto M, Kiyokage E, Toida K, Yoshida T, Miyoshi J, Kamiya H, Takai Y, Sasaki T. Rab3 GTPase-activating protein regulates synaptic transmission and plasticity through the inactivation of Rab3. Proc Natl Acad Sci U S A 2006;103:10029–10034.
71. Müller M, Liu KSY, Sigrist SJ, Davis GW. RIM controls homeostatic plasticity through modulation of the readily-releasable vesicle pool. J Neurosci 2012;32:16574–16585.
72. Weiss N, Sandoval A, Kyonaka S, Felix R, Mori Y, de Waard M. Rim1 modulates direct G-protein regulation of Ca(v)2.2 channels. Pflugers Arch 2011;461:447–459.
73. Han Y, Kaeser PS, Südhof TC, Schneggenburger R. RIM determines Ca^{2+} channel density and vesicle docking at the presynaptic active zone. Neuron 2011;69:304–316.
74. Kaeser PS, Deng L, Wang Y, Dulubova I, Liu X, Rizo J, Südhof TC. RIM proteins tether Ca^{2+} channels to presynaptic active zones via a direct PDZ-domain interaction. Cell 2011;144:282–295.
75. Bustos MA, Lucchesi O, Ruete MC, Mayorga LS, Tomes CN. Rab27 and Rab3 sequentially regulate human sperm dense-core granule exocytosis. Proc Natl Acad Sci U S A 2012;109:E2057–E2066.
76. Tsuboi T, Fukuda M. The Slp4-a linker domain controls exocytosis through interaction with Munc18-1.syntaxin-1a complex. Mol Biol Cell 2006;17:2101–2112.
77. Südhof TC. Function of Rab3 GDP-GTP exchange. Neuron 1997;18:519–522.
78. Fischer von Mollard G, Südhof TC, Jahn R. A small GTP-binding protein dissociates from synaptic vesicles during exocytosis. Nature 1991;349:79–81.
79. Coppola T, Perret-Menoud V, Gattesco S, Magnin S, Pombo I, Blank U, Regazzi R. The death domain of Rab3 guanine nucleotide exchange protein in GDP/GTP exchange activity in living cells. Biochem J 2002;362:273–279.
80. Maycox PR, Link E, Reetz A, Morris SA, Jahn R. Clathrin-coated vesicles in nervous tissue are involved primarily in synaptic vesicle recycling. J Cell Biol 1992;118:1379–1388.
81. Graham ME, Handley MTW, Barclay JW, Ciufo LF, Barrow SL, Morgan A, Burgoyne RD. A gain-of-function mutant of Munc18-1 stimulates secretory granule recruitment and exocytosis and reveals a direct interaction of Munc18-1 with Rab3. Biochem J 2008;409:407–416.
82. Dulubova I, Lou X, Lu J, Huryeva I, Alam A, Schneggenburger R, Südhof TC, Rizo J. A Munc13/RIM/Rab3 tripartite complex: from priming to plasticity? EMBO J 2005;24:2839–2850.
83. Iezzi M, Regazzi R, Wollheim CB. The Rab3-interacting molecule RIM is expressed in pancreatic beta-cells and is implicated in insulin exocytosis. FEBS Lett 2000;474:66–70.
84. Shibasaki T, Sunaga Y, Seino S. Integration of ATP, cAMP, and Ca^{2+} signals in insulin granule exocytosis. Diabetes 2004;53(Suppl 3):S59–S62.
85. Staunton J, Ganetzky B, Nonet ML. Rabphilin potentiates soluble N-ethylmaleimide sensitive factor attachment protein receptor function independently of rab3. J Neurosci 2001;21:9255–9264.
86. Johannes L, Doussau F, Clabecq A, Henry JP, Darchen F, Poulain B. Evidence for a functional link between Rab3 and the SNARE complex. J Cell Sci 1996;109:2875–2884.
87. Henry JP, Johannes L, Dousseau F, Poulain B, Darchen F. Role of Rab3a in neurotransmitter and hormone release: a discussion of recent data. Biochem Soc Trans 1996;24:657–661.
88. Ohya T, Miaczynska M, Coskun U, Lommer B, Runge A, Drechsel D, Kalaidzidis Y, Zerial M. Reconstitution of Rab- and SNARE-dependent membrane fusion by synthetic endosomes. Nature 2009;459:1091–1097.
89. Ohara-Imaizumi M, Nagamatsu S. Insulin exocytotic mechanism by imaging technique. J Biochem 2006;140:1–5.
90. Ohara-Imaizumi M, Fujiwara T, Nakamichi Y, Okamura T, Akimoto Y, Kawai J, Matsushima S, Kawakami H, Watanabe T, Akagawa K, Nagamatsu S. Imaging analysis reveals mechanistic differences between first- and second-phase insulin exocytosis. J Cell Biol 2007;177:695–705.
91. Straub SG, Sharp GWG. Evolving insights regarding mechanisms for the inhibition of insulin release by norepinephrine and heterotrimeric G proteins. Am J Physiol Cell Physiol 2012;302:C1687–C1698.
92. Ohara-Imaizumi M, Nakamichi Y, Tanaka T, Ishida H, Nagamatsu S. Imaging exocytosis of single insulin secretory granules with evanescent wave microscopy: distinct behavior of granule motion in biphasic insulin release. J Biol Chem 2002;277:3805–3808.
93. Ohara-Imaizumi M, Nishiwaki C, Kikuta T, Kumakura K, Nakamichi Y, Nagamatsu S. Site of docking and fusion of insulin secretory granules in live MIN6 beta cells analyzed by TAT-conjugated anti-syntaxin 1 antibody and total internal reflection fluorescence microscopy. J Biol Chem 2004;279:8403–8408.
94. Michael DJ, Xiong W, Geng X, Drain P, Chow RH. Human insulin vesicle dynamics during pulsatile secretion. Diabetes 2007;56:1277–1288.
95. Shibasaki T, Takahashi H, Miki T, Sunaga Y, Matsumura K, Yamanaka M, Zhang C, Tamamoto A, Satoh T, Miyazaki J-I, Seino S. Essential role of Epac2/Rap1 signaling in regulation of insulin granule dynamics by cAMP. Proc Natl Acad Sci U S A 2007;104:19333–19338.
96. Lin C-C, Huang C-C, Lin K-H, Cheng K-H, Yang D-M, Tsai Y-S, Ong R-Y, Huang Y-N, Kao L-S. Visualization of Rab3A dissociation during exocytosis: a study by total internal reflection microscopy. J Cell Physiol 2007;211:316–326.
97. Larijani B, Hume AN, Tarafder AK, Seabra MC. Multiple factors contribute to inefficient prenylation of Rab27a in Rab prenylation diseases. J Biol Chem 2003;278:46798–46804.
98. Tiwari S, Italiano JE, Barral DC, Mules EH, Novak EK, Swank RT, Seabra MC, Shivdasani RA. A role for Rab27b in NF-E2-dependent pathways of platelet formation. Blood 2003;102:3970–3979.

99. Coppola T, Frantz C, Perret-Menoud V, Gattesco S, Hirling H, Regazzi R. Pancreatic beta-cell protein granuphilin binds Rab3 and Munc-18 and controls exocytosis. Mol Biol Cell 2002;13:1906–1915.
100. Gomi H, Mizutani S, Kasai K, Itohara S, Izumi T. Granuphilin molecularly docks insulin granules to the fusion machinery. J Cell Biol 2005;171:99–109.
101. Fukuda M. Versatile role of Rab27 in membrane trafficking: focus on the Rab27 effector families. J Biochem 2005;137:9–16.
102. Kimura T, Niki I. Rab27a, actin and beta-cell endocytosis. Endocr J 2011;58:1–6.
103. Kimura T, Taniguchi S, Niki I. Actin assembly controlled by GDP-Rab27a is essential for endocytosis of the insulin secretory membrane. Arch Biochem Biophys 2010;496:33–37.
104. Göpel S, Zhang Q, Eliasson L, Ma X-S, Galvanovskis J, Kanno T, Salehi A, Rorsman P. Capacitance measurements of exocytosis in mouse pancreatic alpha-, beta- and delta-cells within intact islets of Langerhans. J Physiol (Lond) 2004;556:711–726.
105. Allersma MW, Bittner MA, Axelrod D, Holz RW. Motion matters: secretory granule motion adjacent to the plasma membrane and exocytosis. Mol Biol Cell 2006;17:2424–2438.